FAST.Farm Response to Varying Wind Inflow Techniques

Kelsey Shaler*, Jason Jonkman†, Paula Doubrawa‡, and Nicholas Hamilton§
National Renewable Energy Laboratory, Golden, CO 80401, USA

FAST.Farm is a newly developed multiphysics, midfidelity engineering tool that can be used to predict turbine power and structural loads of wind turbines in a wind farm. Previous studies have shown the similarities and differences between FAST.Farm and large-eddy simulations (LES) using the same LES-precursor-generated ambient wind inflow. The ability to generate ambient wind inflow using a synthetic turbulence engineering model (e.g., TurbSim or the Mann model), which are more easily generated than LES precursors, has recently been integrated into FAST.Farm. This work aims to: 1) assess the differences in turbine and wake response resulting from various wind-inflow generation techniques, and 2) establish guidelines by which a synthetic turbulent inflow should be generated for wind farm analysis. It was found that properly setting spatial coherence parameters for the transverse wind velocity components is necessary to accurately predict wake meandering. TurbSim-generated inflow can be used in FAST.Farm to accurately predict thrust, power, speed, and torque for waked and unwaked turbines; wake meandering behavior across different atmospheric conditions; and averaged wake-deficit advection and evolution effects.

I. Nomenclature

L	=	Length scale
σ	=	Standard deviation of time series
f	=	Frequency
S	=	Scaling factor
$Coh_{i,j}$	=	Magnitude patial coherence between points i and j
a	=	Coherence decrement parameter
b	=	Coherence offset parameter
r	=	distance between points i and j
$\overline{u_{\text{hub}}}$	=	mean hub height wind speed
K	=	u-, v-, and w-velocity components

II. Introduction

In the context of wind farm design and optimization, it is crucial to be able to perform thousands of wind-farm-scale simulations in near real time. FAST.Farm is a new midfidelity tool developed by the National Renewable Energy Laboratory (NREL) for this purpose. As an extension of the widely used OpenFAST software, FAST.Farm aims to model the wake physics of wind farms for the purpose of accurately and efficiently predicting wind turbine power production and structural loading. In past work, FAST.Farm wake-related input parameters were calibrated against high-fidelity large-eddy simulations (LES) implemented in the Simulator fOr Wind Farm Applications (SOWFA) [1] and later validated against SOWFA simulations [2] for different inflow and control conditions. In both calibration and validation of FAST.Farm, ambient wind data was generated with a high-fidelity LES precursor simulation common to both FAST.Farm and SOWFA. The validation study showed that FAST.Farm is able to reproduce statistical distributions of wind turbine generator power, torque, rotor thrust, and rotor speed for single- and three-turbine configurations modeled with SOWFA. Additionally, lateral and vertical wake meandering as well as wake-deficit advection, evolution, and merging were accurately predicted for most cases. Although these results are promising, a new option of including

*Post-Doctoral Researcher, National Wind Technology Center, kelsey.shaler@nrel.gov
†Senior Engineer, National Wind Technology Center, AIAA Professional Member
‡Research Engineer, National Wind Technology Center
§Research Engineer, National Wind Technology Center

ambient wind inflow using a synthetic turbulence engineering model (e.g., TurbSim [3] or the Mann model) has recently been integrated into FAST.Farm, which would theoretically allow for quicker ambient wind generation and ease of manipulating spatial and temporal discretizations within FAST.Farm.

This work aims to complement previous FAST.Farm studies by comparing four methods of modeling the inflow wind conditions. The purpose of these studies is to assess the differences in turbine and wake response to the wind-inflow generation method and establish the importance of accurately modeling certain inflow parameters. Guidelines for producing TurbSim inflow for use in FAST.Farm simulations are also established. Though this paper will refer to TurbSim-generated inflow, in a broader sense it applies to synthetic turbulence generated using a Kaimal spectrum with exponential coherence. These guidelines could also be applied to a range of inflow-generation techniques and tailored to LES or experimental results.

III. Approach and Methods

This section provides an overview of FAST.Farm, followed by descriptions of all modeling cases that will be used in this study.

A. Overview of FAST.Farm

FAST.Farm is a multiphysics engineering tool that accounts for wake interaction effects on turbine performance and structural loading in wind farm applications. FAST.Farm is an extension of the NREL software OpenFAST, which solves the aero-hydro-servo-elasto dynamics of individual turbines. FAST.Farm extends this analysis to include wake deficits, advection, deflection, meandering, and merging for wind farms. FAST.Farm is based on the dynamic wake meandering (DWM) model [4], but expands on it to address many limitations of past DWM implementations. Using this method, the wake deficit of each turbine is computed using the steady-state thin-shear layer approximation of the Navier-Stokes equations and the wake is perturbed with a turbulent freestream to capture wake meandering. Wake merging is modeled using a superposition method. As in OpenFAST, rotor aerodynamics are modeled using the blade-element momentum (BEM) theory with options for advanced corrections, including unsteady aerodynamics. The FAST.Farm implementation of DWM is an improvement over past implementations primarily because of:

1) Optional use of LES-generated precursors for ambient wind
2) Improvement of wake advection, deflection, and merging
3) Optional inclusion of a wind-farm-wide super controller
4) Ability to solve the entire wind farm using parallelization of the computations
5) Calibration of wake-related model parameters against SOWFA simulations.

A complete description of FAST.Farm theory and implementation is available in [5] and [6].

B. Modeling Cases

Several modeling cases are run to compare ambient wind inflow generated synthetically by TurbSim to inflow generated from a high-fidelity LES precursor using the atmospheric boundary layer (ABL) solver of SOWFA without wind turbines present [7]. All cases considered in this work are presented in this section.

For this study, wind farm simulations using four different wind-inflow generation techniques are compared. These wind-inflow techniques include LES-generated inflow and three TurbSim-generated inflow methods. The same cases that were run for the FAST.Farm validation [2] are run again here and summarized in Table 1. For all cases, the main flow direction is oriented along the X-axis, with the Y- and Z- coordinates corresponding to the transverse and wall-normal components of velocity, respectively. All simulations are run for 1700 seconds, not including a 300-s initial transient period. The wake discretization in FAST.Farm consists of 140 wake planes per rotor, each with a radial finite-difference grid of 40 nodes with a spacing of 5 m. The wind turbine properties match those of the NREL 5-MW reference turbine [8], except for the elimination of shaft tilt and a rigidly modeled turbine (other than the variable-speed rotor degree of freedom).

The freestream precursor flow fields, detailed in Section III.C, are used as inflow for the FAST.Farm simulations described in Table 1. These flow fields are composed of low- and high-resolution domains. The low-resolution domain encompasses the entire wind farm in order to resolve wake meandering and merging. This domain has a spatial resolution of 10 m and a temporal resolution of 2 s. The high-resolution domains encompass each individual turbine and are primarily considered for turbine aero-elastic excitation. These domains have a spatial resolution of 10 m and a temporal resolution of $1/3$ s.

Table 1 Case description for wind inflow comparison.

Case Name	Number of Turbines	Turbine Spacing	Hub-Height Mean Wind Speed	Turbulence Intensity	Shear Exponent	Yaw Error
V6_TI8_1WT	1	−−	6 m/s	8%	0.2	0°
V8_TI10_1WT_YAW	1	−−	8 m/s	10%	0.2	15°
V8_TI6_1WT_YAW	1	−−	8 m/s	6%	0.1	10°
V8_TI10_3WT	3	8D	8 m/s	10%	0.2	0°
V8_TI10_3WT_YAW	3	8D	8 m/s	10%	0.2	10°/10°/0°
V8_TI6_3WT	3	8D	8 m/s	6%	0.1	0°

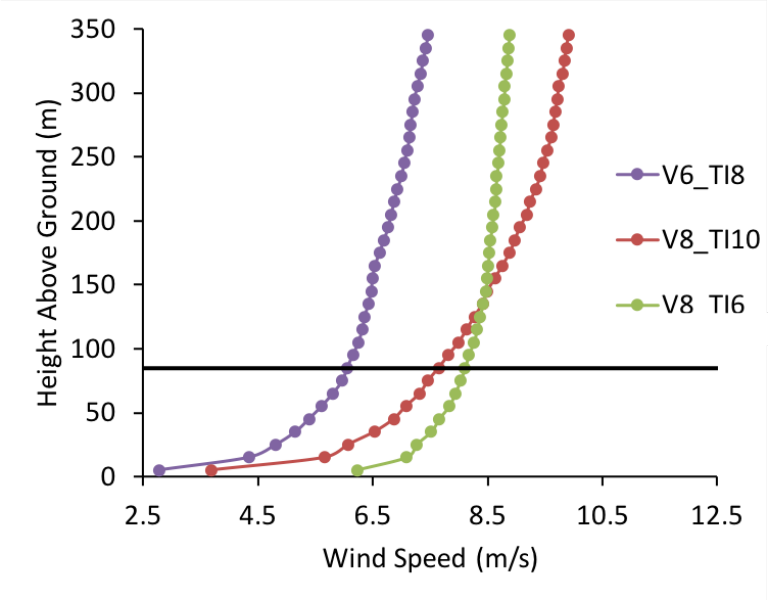

Fig. 1 Wind inflow velocity profiles for each inflow condition. Hub height is indicated by the black horizontal line.

C. Wind Inflow

Three sets of precursor wind-inflow data are required for the six FAST.Farm cases:

- V6_TI8: 6 m/s mean hub height wind speed, 8% turbulence intensity (TI), and a power-law shear exponent of 0.2
- V8_TI10: 8 m/s, 10% TI, and a shear exponent of 0.2
- V8_TI6: 8 m/s, 6% TI, and a shear exponent of 0.1.

Precursor data sets were generated using each wind-inflow technique. One set was generated using LES, which creates wind-inflow conditions that are three-dimensional in space (plus time). Three sets were generated using TurbSim, which creates two-dimensional (plus time) turbulent flow fields. A three dimensional flow field is estimated from planar flow data by propagating the planes at the mean wind speed using Taylor's frozen-turbulence assumption. For the LES-generated inflow cases, each precursor is generated on an $X \times Y \times Z = 5$ km $\times$ 2 km $\times$ 0.35 km domain. The LES-generated inflow was also used in LES actuator-line model (ALM) simulations of the wind turbines using SOWFA-ALM. For the TurbSim inflow cases, TurbSim v2 [3] was used, with turbulence generated on an $Y \times Z = 2$ km $\times$ 0.35 km domain tuned to match a specified time-averaged wind profile from the LES-generated inflow, shown in Fig. 1.

The first set of TurbSim cases (TS_SPECTRA) was computed by specifying the u-, v-, and w-velocity spectra following

Eq. (1) to match the International Electrotechnical Commission (IEC) Kaimal turbulence spectrum [9],

$$PSD_K = \left\{ \frac{(4L_K)/(\overline{u_{\text{hub}}})\sigma_K^2}{1 + (6fL_K/\overline{u_{\text{hub}}})} \right\}^{5/3} \tag{1}$$

where PSD_K is the power spectral density (PSD) at a given frequency, f, for $K = u, v, w$ velocity components; L_K is the IEC 61400-1 standard length scale; $\overline{u}_{\text{hub}}$ is the mean hub height wind speed; and σ_K is the standard deviation of the fluctuating velocity component K. For each inflow case, σ_K is computed at hub height from the LES-generated inflow velocity. When the wind velocity time series is generated by TurbSim based on this spectra, the standard deviations of the velocity components at hub height are close, but not identical, to those from the LES-generated inflow. Therefore, to ensure the same level of turbulence, the u-, v-, and w-velocity PSDs at the hub height were scaled in TurbSim to match those from the LES-generated inflow, following Eq. (2).

$$S_K = \frac{\sigma_{K,\text{TS}}^2}{\sigma_{K,\text{ABL}}^2} \tag{2}$$

Here, $\sigma_{K,\text{ABL}}$ and $\sigma_{K,\text{TS}}$ are the standard deviations of the K-velocity wind component at hub height in the LES-generated and spectra-specified TurbSim inflow, respectively; and S_K is the scaling factor used to match $\sigma_{K,\text{TS}}$ to $\sigma_{K,\text{ABL}}$. Despite these similarities, the actual time history varies dramatically from the LES-generated inflow because of the random selection of the phases of the frequency components from a uniform distribution based on the turbulence seeds.

A second set of TurbSim inflow files (TS_ModSpectra) was generated based on the first TurbSim method by additionally specifying a spectra frequency cutoff to approximately match that of the LES-generated inflow. This cutoff frequency is dictated by the resolution of the LES computation, but does not reflect the expected spectra from real atmospheric turbulence.

In an attempt to alleviate the phasing differences between SOWFA- and TurbSim-generated inflow, a third set of TurbSim inflow files (TS_TimeSeries) was generated in which the wind-inflow u-, v-, and w-velocity time series from the LES-generated inflow at the most upstream wind turbine hub was specified directly in TurbSim, thus prescribing the phases of the frequency components. At other points in the domain, the wind time series is derived from exponential spatial-coherence functions. This allows for closer statistical agreement between TurbSim- and LES-generated inflow files, while still testing the differences between the inflow techniques.

Statistical variation between inflow velocity cases are shown through a comparison of hub height velocity for all wind inflow techniques in terms of probability density functions (PDFs) is shown in Fig. 2. Overall, there is good agreement between all inflow techniques. As expected, the TS_Spectra and TS_ModSpectra results are Gaussian because of the random selection of frequency component phases from a uniform distribution. The TS_ModSpectra results exhibit a slightly higher peak centered around the respective mean velocity because the frequency cutoff in the modified spectra leads to a slightly reduced level of turbulence. The ABL and TS_TimeSeries results are skewed from a Guassian distribution, suggesting a slightly nonuniform distribution of phases. Moreover, the ABL and TS_TimeSeries results are expected to overlap, because the hub height velocities are equivalent. This is true for most cases, though there is a small difference in the mean v- and w-velocity components for V8_TI10. This is because of the small nonzero mean value of these components for the LES-generated inflow. In contrast, TurbSim forces these values to be identically 0 unless a wind direction or veer angle are explicitly specified, which they are not for the current test cases.

Wind inflow PSD comparisons for all wind inflow techniques for a point at hub height are shown in Fig. 3. The PSDs for ABL and TS_TimeSeries results clearly show the cutoff frequency and are nearly identical following the similarity between the respective time series. For low-frequency content, TS_Spectra and TS_ModSpectra results are in close agreement to the ABL and TS_TimeSeries results and nearly identical to each other. However, TS_Spectra and TS_ModSpectra results deviate for high-frequency content because of the imposed frequency cutoff for TS_ModSpectra. By default, the IEC Kaimal spectra result in higher energy content at high frequencies. When FAST.Farm cases were compared using TS_Spectra and TS_ModSpectra wind inflow, negligible differences were found between the resulting wake response because wake meandering is driven by low-frequency turbulence. Therefore, tailoring of the velocity spectra to the LES cutoff frequency is not necessary and further results using the TS_ModSpectra wind inflow are not shown in this paper.

Apart from the hub height point, TurbSim generates wind velocities at other points using u-, v-, and w-spatial-coherence models based on a selection of coherence model equations and their associated parameters. These models and parameters can either be specified explicitly or left as *default* values in TurbSim. When the IEC spatial-coherence

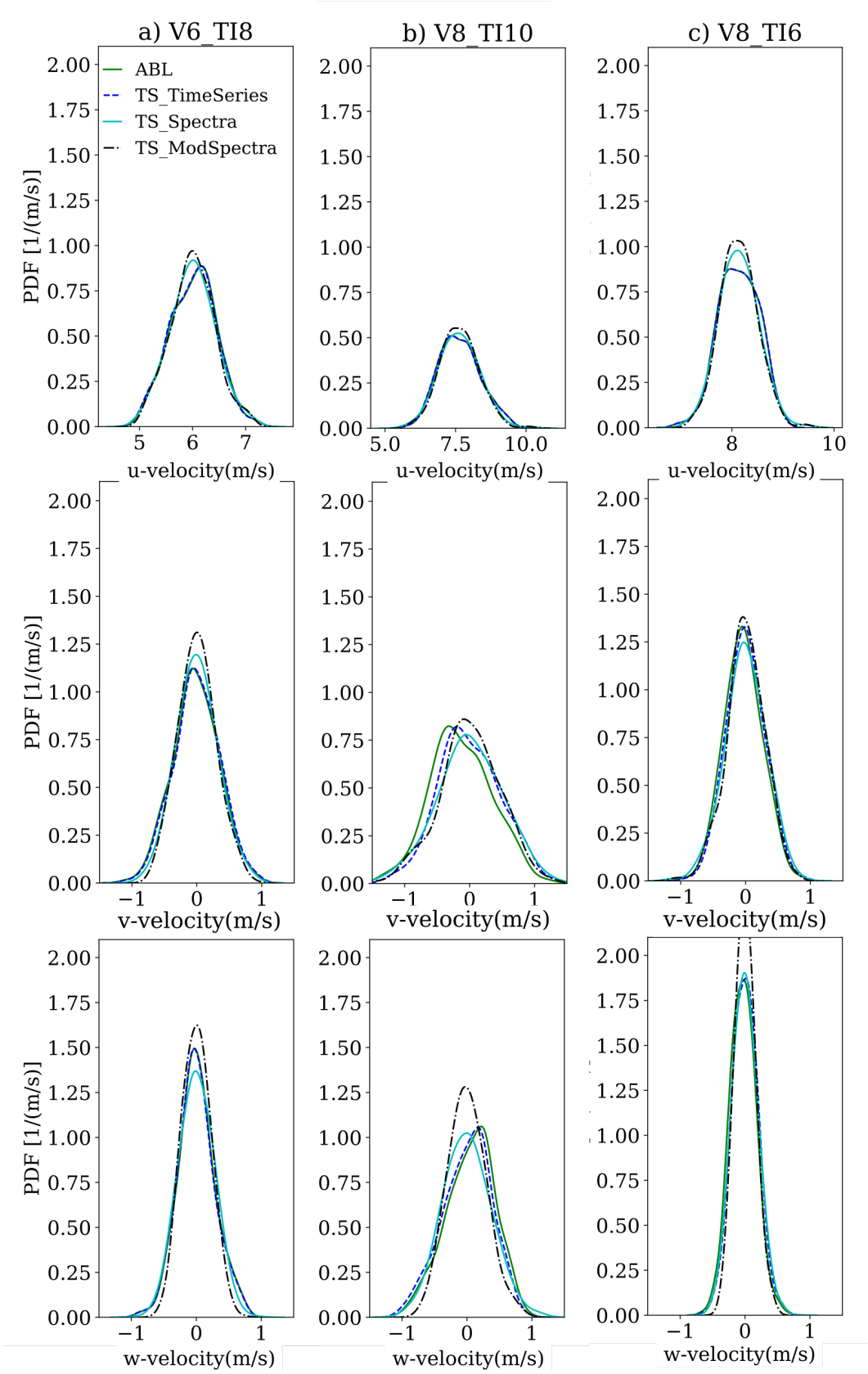

Fig. 2 PDF comparisons of hub height velocity for all wind inflow techniques for (a) V6_TI8, (b) V8_TI10, and (c) V8_TI6.

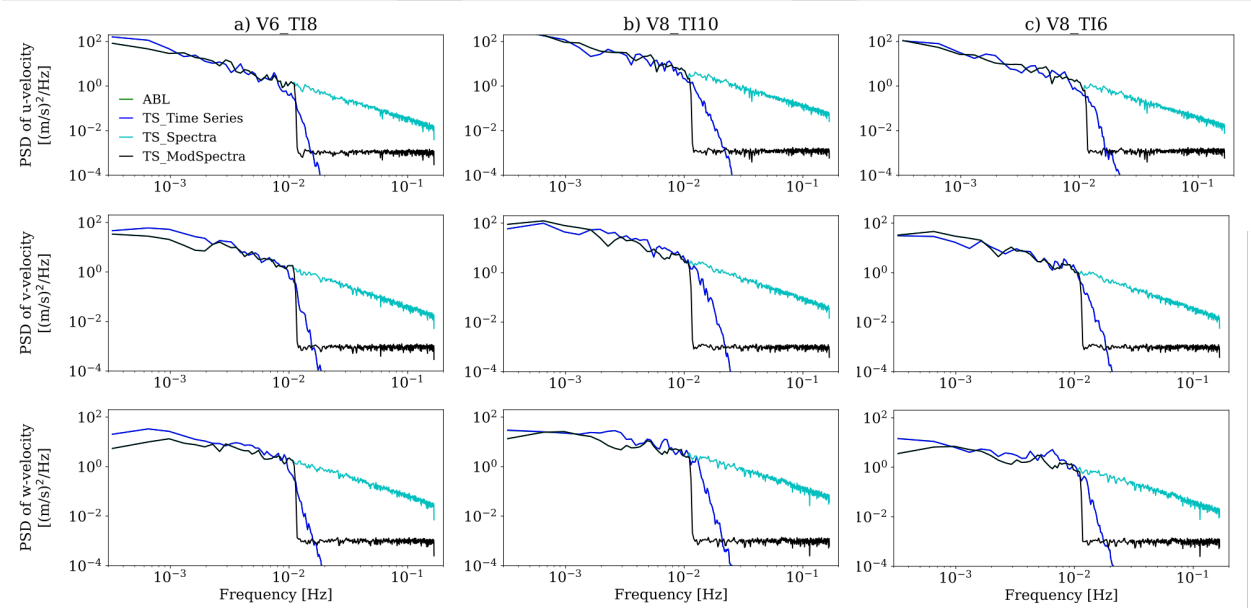

Fig. 3 Wind inflow PSD comparisons for all wind inflow techniques for (a) V6_TI8, (b) V8_TI10, and (c) V8_TI6.

model is selected, spatial coherence is computed using Eq. (3) [3].

$$Coh_{i,j_K} = exp\left(-a_K\sqrt{\left(\frac{fr}{\overline{u}_{\text{hub}}}\right)^2 + (rb_K)^2}\right) \tag{3}$$

where Coh_{i,j_K} is the spatial coherence between points i and j for the velocity components $K = u, v, w$; r is the distance between points i and j; a_K is the coherence decrement parameter; and b_K is the coherence offset parameter. It was discovered during the course of this work that the use of the IEC coherence model with default coherence parameters together with the IEC Kaimal spectra results in negligible wake meandering. This is because the default v- and w-coherence parameters in TurbSim are set such that $b_K = 0$ and a_K is a very large number, effectively resulting in no coherence ($Coh_{i,j_K} = 0$) [3]. In addition to reduced agreement with physical wake meandering and LES-generated inflow, this lack of meandering can result in a severe and nonphysical reduction of downstream turbine thrust and associated response. Instead of using the default values, the v- and w-coherence parameters were specified to identically equal the u-coherence parameters specified in the IEC standard ($a_K = 12.0$ and $b_K = 0.00035273$ m^{-1}) [3]. A comparison of inflow wind spatial (magnitude-square) coherence between LES-generated inflow and Eq. (3) squared (used for all TurbSim-generated inflow) is shown in Fig. 4. Coherence is an indicator of the similarity of energy content at two points in space, with a higher coherence value indicating greater similarity. Point separations of $0.5D$ and $1D$ are considered. The reported coherence from the LES was computed by taking the average of coherence values at several lateral locations spanning the hub height and the full width of the domain. For both distances, the IEC standard identifies higher coherence at low frequencies than calculated by LES. At higher frequencies, the nonzero floor of the LES-generated inflow coherence results from numerical noise in the coherence calculation and is thus unphysical. Postprocessing of the TurbSim-generated inflow time series would yield a similar nonzero offset. Although no attempt was made to calibrate the coherence model parameters to the LES coherence at low frequencies, this step could be pursued in future work. IEC-standard coherence does not reach unity at 0 Hz because of the inclusion of the offset parameter, b_K.

Note that when wake dynamics are included in a FAST.Farm simulation, it is necessary to extend the vertical domain well above the top of the rotor plane to accommodate vertical wake meandering. Thus, when TurbSim-generated inflow is used, it is necessary to specify the hub height in TurbSim to be higher than the actual hub height due to the way the planar grid is specified. The specified TurbSim 'hub height' is then used as the wind speed reference height in defining the spatial coherence in the IEC model and the advection of the frozen turbulence in FAST.Farm. However,

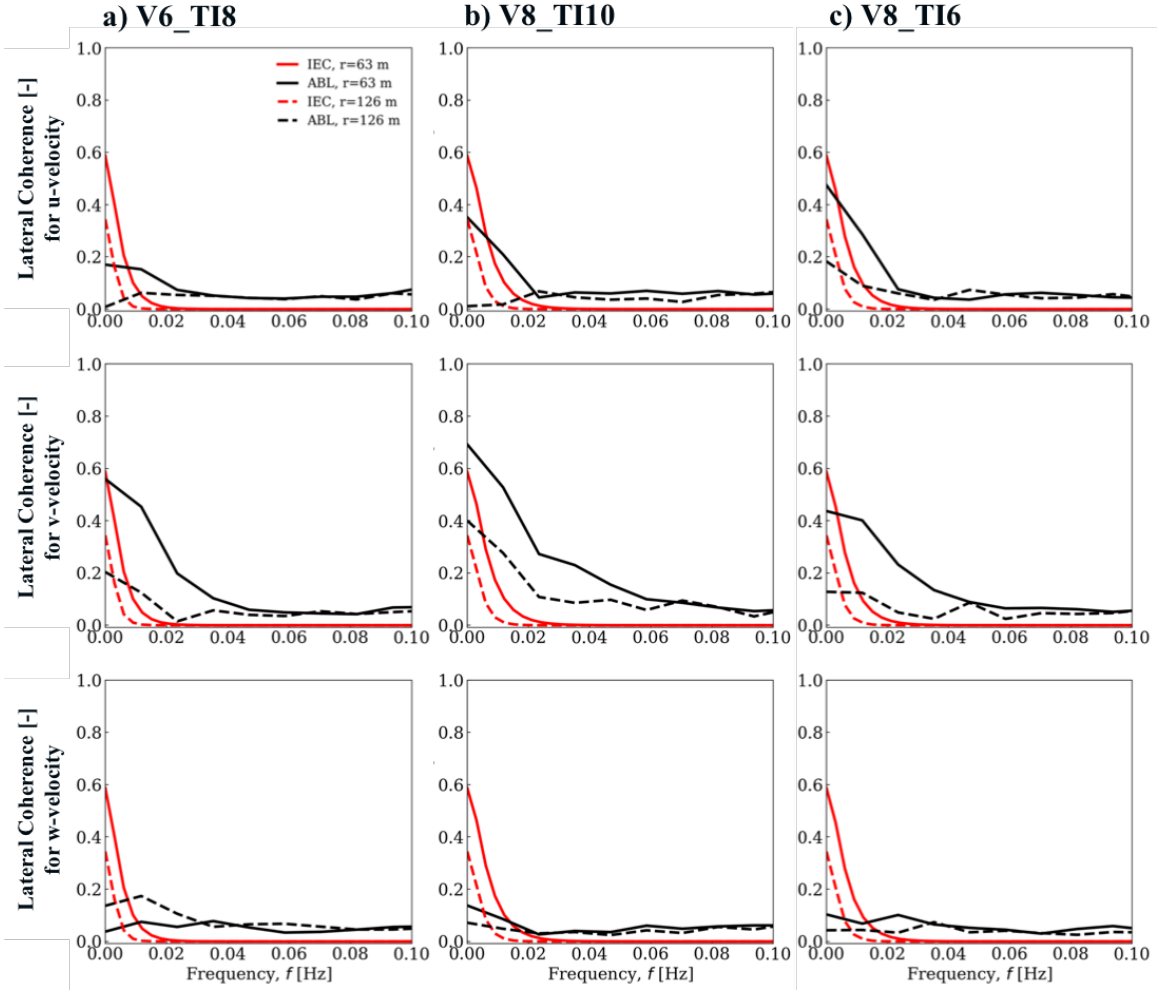

Fig. 4 Wind inflow coherence comparisons for various wind inflow techniques for (a) V6_TI8, (b) V8_TI10, and (c) V8_TI6.

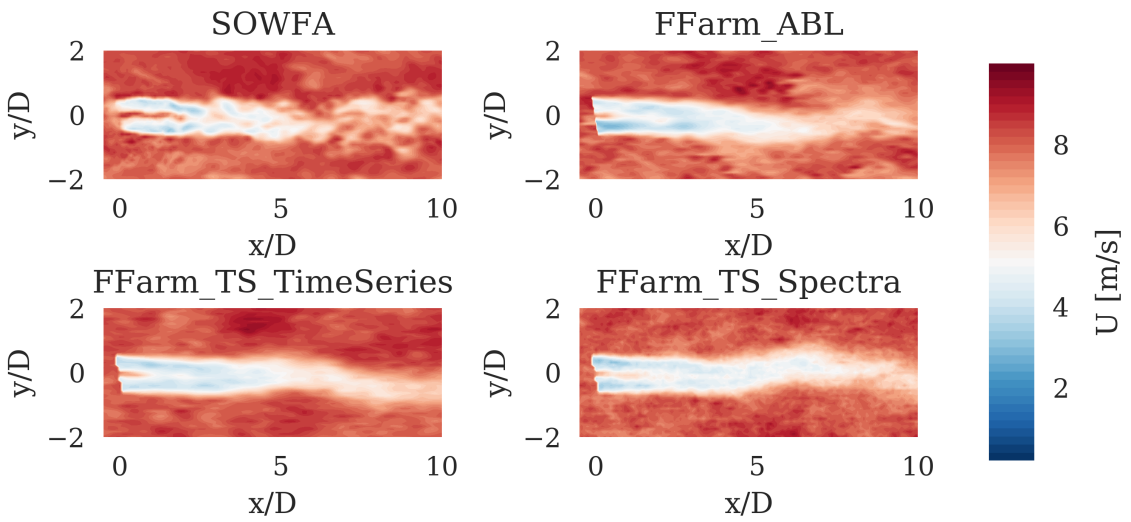

Fig. 5 Instantaneous flow visualization of XY planes from all inflow methods for Case V8_TI6_1WT_Yaw.

these parameters should be based on the actual hub height velocity. To address this issue, TurbSim should be changed in the future so that the hub height input is decoupled from the specification of the planar grid.

IV. Results

This section discusses the results of the wind-inflow comparison studies. FAST.Farm results from the various wind-inflow generation techniques are compared to LES results. Wake formation and propagation differences are qualitatively studied by comparing instantaneous slices of the flow along XY planes slicing through the hub center. YZ slices are also compared at locations $2D$ downstream of each turbine. Turbine response differences are quantitatively assessed by comparing time series and statistical results of thrust, generator power, rotor speed, and generator torque. Wake development differences are quantitatively studied by comparing time series and statistical results for lateral and vertical wake center positions at various distances downstream of each turbine, as well as axial wake deficits at several downstream distances. Because SOWFA and FFarm_ABL results have previously been compared [2], the discussion here is focused on the comparisons with TurbSim-generated inflow.

A. Flow Visualization

Instantaneous flow visualizations of the XY planes for Cases V8_TI6_1WT_Yaw and V8_TI6_3WT are shown in Figs 5 and 6, respectively. The ambient flow outside the wake compares well between the SOWFA, FFarm_ABL, and FFarm_TS_TimeSeries simulations, with similar large-scale structures visible in Fig. 5. Similarity is expected between the SOWFA and FFarm_ABL simulations, as the same inflow is used. High agreement with FFarm_TS_TimeSeries indicates that Taylor's frozen-turbulence assumption holds well when turbulence intensity is low. Inflow cases exhibit greater differences in the wake region, though all results feature comparable wake velocity deficit magnitudes, wake deflection, and wake extent. In the wake region, SOWFA simulations include mesh refinement leading to finer resolution as compared to the FAST.Farm results because FAST.Farm does not require wake refinement. The FAST.Farm solutions with TurbSim-generated inflow appear to have smoother wakes than in the FFarm_ABL simulation, which is more significant in multiturbine simulations, as shown in Fig. 6. These differences are more apparent in YZ plane visualizations. Instantaneous flow visualizations of YZ planes $2D$ downstream from WT1 and WT2 for Cases V8_TI10_3WT and V8_TI6_3WT are shown in Figs. 7 and 8, respectively. This appearance of a smoother wake seen in TurbSim-generated inflow simulations is likely caused by the lack of mesh refinement in FAST.Farm and differences in the ambient background flow as a result of the use of IEC spatial coherence in TurbSim-generated inflow, rather than differences in the wakes themselves. In the YZ planes, the flow outside the wake is consistent between the SOWFA and FFarm_ABL results, with greater differences for FFarm_TS_TimeSeries and FFarm_TS_Spectra attributed to the IEC spatial-coherence model.

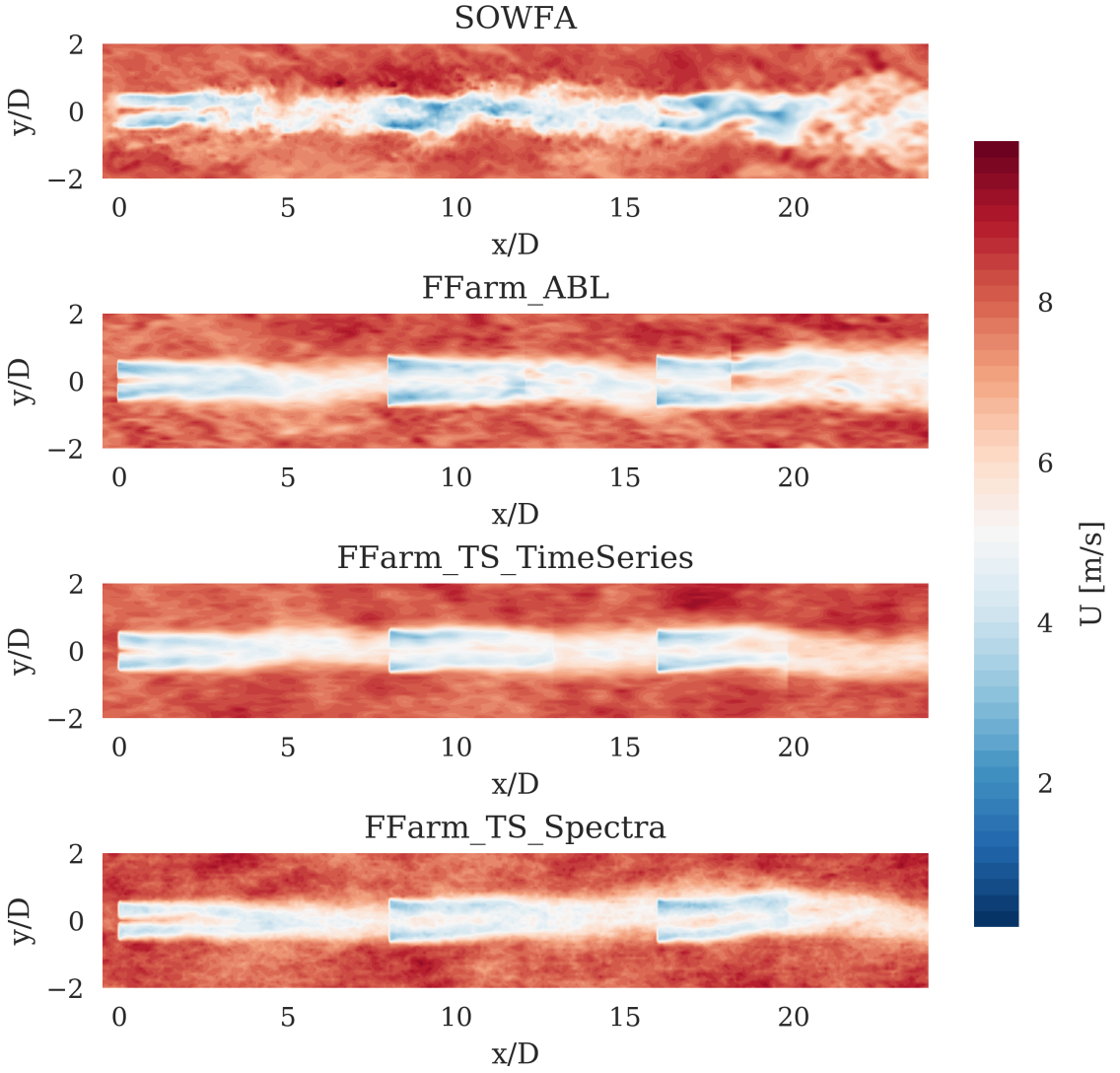

Fig. 6 Instantaneous flow visualization of XY planes from all inflow methods for Case V8_TI6_3WT.

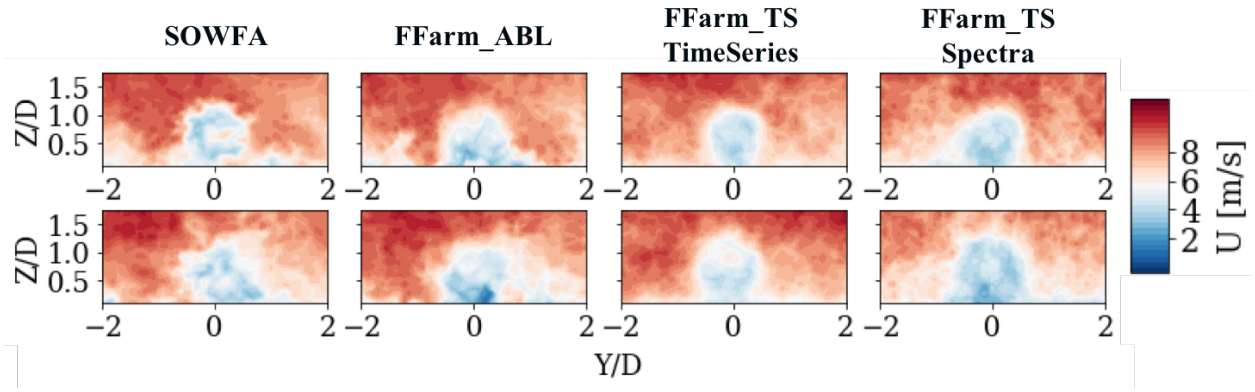

Fig. 7 Instantaneous flow visualization of the YZ planes located $2D$ downstream from WT1 (top) and WT2 (bottom) from all inflow methods for Case V8_TI10_3WT.

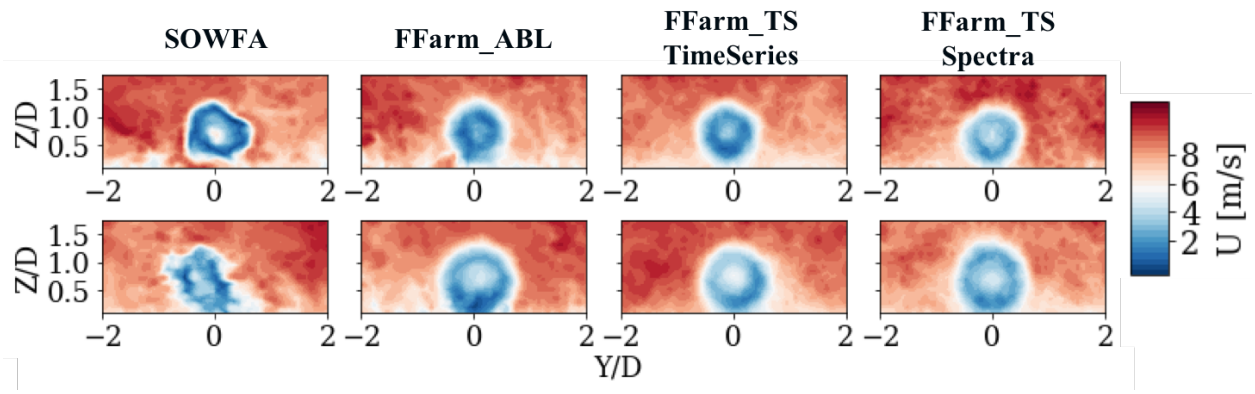

Fig. 8 Instantaneous flow visualization of the YZ planes located $2D$ downstream from WT1 (top) and WT2 (bottom) from all inflow methods for Case V8_TI6_3WT.

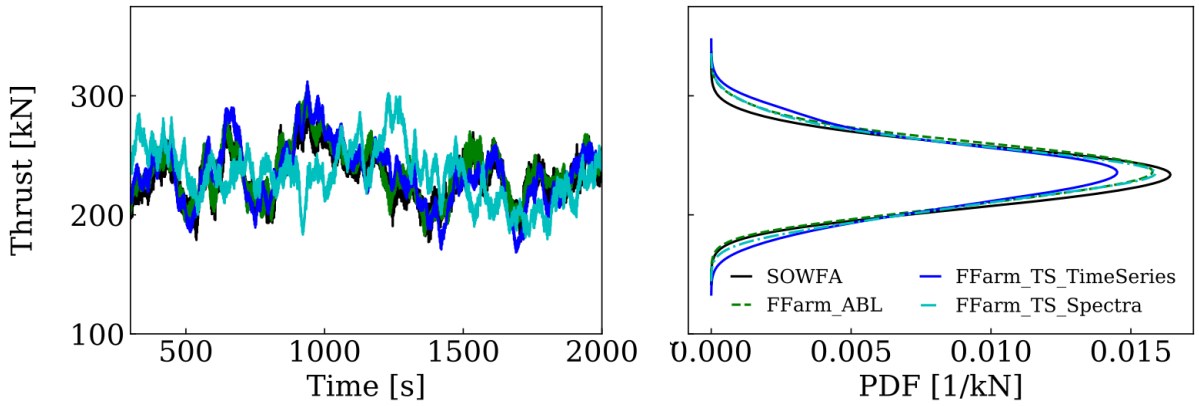

Fig. 9 PDF (left) and time series (right) of rotor thrust for Case V6_TI8_1WT.

B. Turbine Response

Time series and PDF results of the aerodynamic applied rotor thrust for Cases V6_TI8_1WT and V8_TI10_3WT are shown in Fig. 9 and 10, respectively. Note that the PDF results use larger and fewer bins than the equivalent figures from [2], resulting in smoother PDFs that are more statistically converged. Rotor thrust is the primary driver of wake deficits; it is therefore essential to accurately predict rotor thrust to accurately predict wake effects in a wind farm. For both cases, the time series of SOWFA, FFarm_ABL, and FFarm_TS_TimeSeries are quite consistent with each other. This is expected since the SOWFA and FFarm_ABL simulations use the same ambient inflow and the FFarm_TS_TimeSeries have the same velocity time series at the hub height of WT1. As expected, the time series are quite different for the FFarm_TS_Spectra results. Statistically, however, the mean rotor thrust from all inflows compares well for WT1. For Case V6_TI8_1WT, agreement between FFarm_ABL and FFarm_TS_Spectra results are nearly statistically identical, with slightly higher variance than the SOWFA results. Further, increased variance is seen in the FFarm_TS_TimeSeries results, which was not expected; however, considering the consistent time series, this suggests that the PDF results are highly sensitive to the level of statistical significance in the results (i.e., the longer the time series, the more consistent the PDF results will become). A greater degree of variation is observed between inflow methods for the multiturbine simulations, as shown in Fig. 10. Similar agreement between methods is seen for WT1, but differences develop for WT2 and WT3. The time series results are comparable to those for WT1, though reduced mean thrust is evident for downstream turbines. Statistically, closer agreement is seen between FFarm_ABL and FFarm_TS_TimeSeries further downstream, with increased variance of the turbines' response resulting from FFarm_TS_Spectra inflow. A lower mean thrust is seen for all FAST.Farm results as compared to SOWFA results.

Time series and PDF results of the generator power for Cases V8_TI10_3WT and V8_TI10_3WT_Yaw are

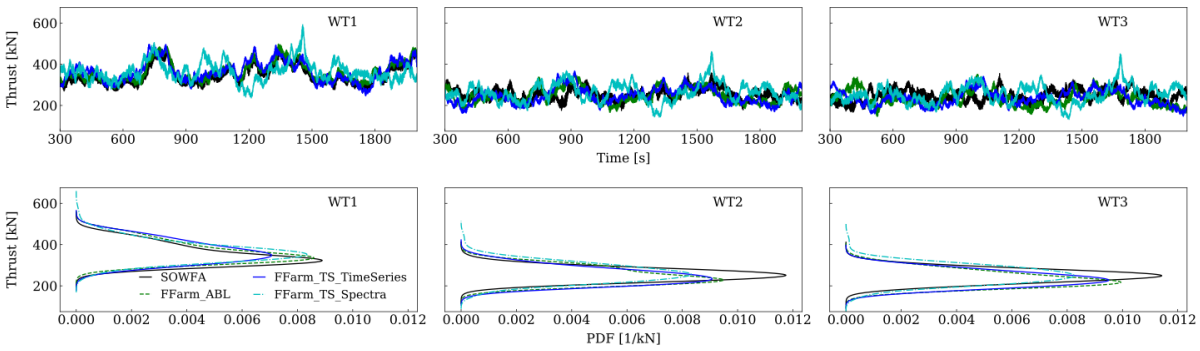

Fig. 10 Time series (top) and PDF (bottom) of rotor thrust for Case V8_TI10_3WT.

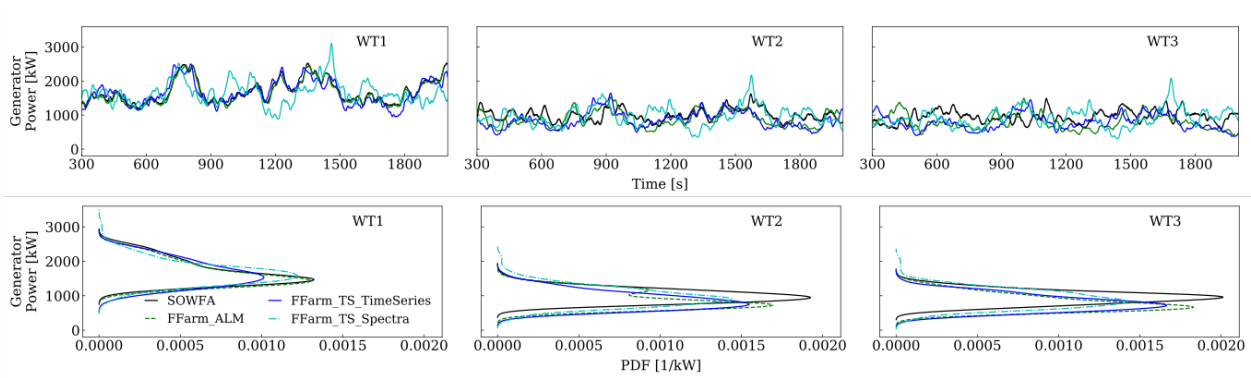

Fig. 11 Time series (top) and PDF (bottom) of generator power for Case V8_TI10_3WT.

shown in Figs. 11 and 12, respectively. As with rotor thrust, generator power time series resulting from FFarm_ABL and FFarm_TS_TimeSeries simulations closely match SOWFA results, with greater differences resulting from the FFarm_TS_Spectra inflow. For all FAST.Farm simulations, downstream wind turbines show greater deviation from the results provided by SOWFA. PDF results of the generator torque and rotor speed for Case V8_TI10_3WT are shown in Fig. 13 and reveal similar trends.

C. Wake Meandering

Time series of the lateral (Y) and vertical (Z) wake center positions between $2D$ and $8D$ downstream of the wind turbine in $2D$ intervals are shown in Fig. 14 for Case V8_TI10_1WT_Yaw.

Small wake deficit velocities and highly asymmetric velocity fields contribute to the uncertainty in wake center detection, resulting in numerical 'spikes' [10]. In general, FFarm_ABL results compare well with SOWFA results. There are greater differences in transient wake location when comparing FFarm_TS_TimeSeries and FFarm_TS_Spectra results. However, all methods capture the same general trends for both lateral and vertical wake meandering. FFarm_TS_TimeSeries does not result in the same wake meandering as FFarm_ABL, even though the u-, v-, w-velocity time series at the hub are identical in both cases. This further confirms that the spatial coherence is very important to the meandering. The propagation of wake features downstream is observed in the wake center plots from $2D$ to $8D$. Though the characteristics of these features differ between inflow techniques, this indicates that the wake-advection speed is similar both between SOWFA and FAST.Farm simulations and between LES-generated and TurbSim-generated inflow, further validating the Taylor's frozen-turbulence assumption.

PDF results of the lateral and vertical wake center positions for Cases V8_TI10_3WT and V8_TI6_3WT are shown in Figs. 15 and 16, respectively. Results are shown from $2D$ to $8D$ downstream for each wind turbine in $2D$ intervals, omitting the planes slicing through WT2 and WT3. The planes slicing through WT2 and WT3 are not shown because the wake propagation calculation for each wind turbine in FAST.Farm initiates at the rotor plane, resulting in nonphysical wake effects at that plane. Despite differences in the wake-meandering time series, lateral wake meandering statistics

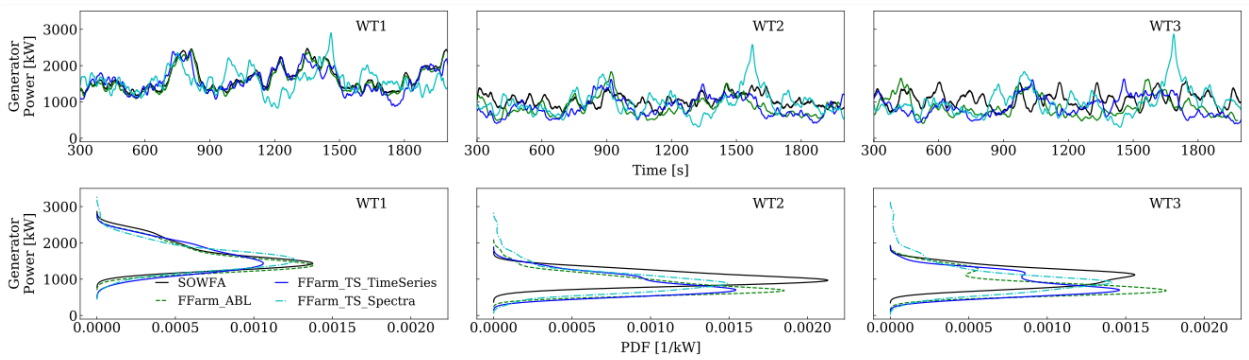

Fig. 12 Time series (top) and PDF (bottom) of generator power for Case V8_TI10_3WT_YAW.

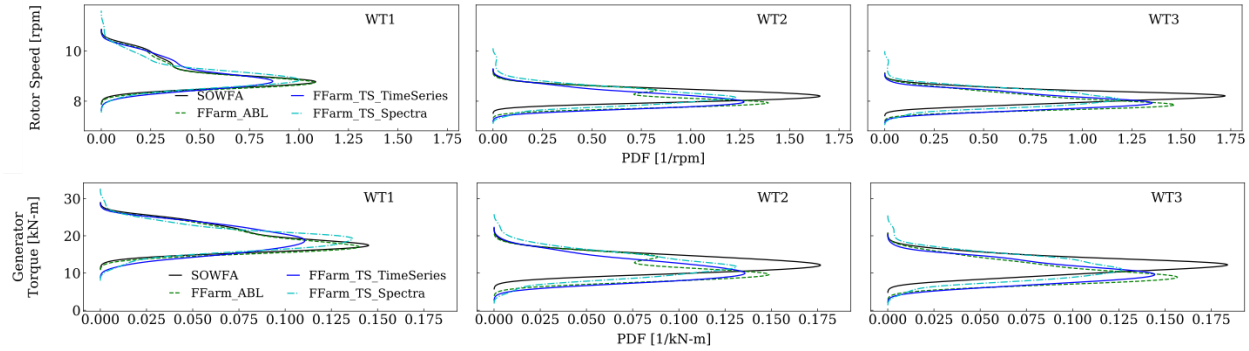

Fig. 13 PDF of rotor speed (top) and generator torque (bottom) for Case V8_TI10_3WT.

are very consistent for Case V8_TI10_3WT results between both TurbSim-generated simulations for both cases, with only small differences from the FAST.Farm simulation using LES-generated inflow. Similar findings are shown for vertical meandering, though the mean wake location is generally lower in FAST.Farm results than SOWFA results.

D. Wake Deficits

Radial profiles of the azimuth and temporal averages of the axial wake deficits in the meandering frame of reference from $2D$ to $8D$ downstream of each turbine in $2D$ intervals for Cases V8_TI10_3WT and V8_TI6_3WT are shown in Figs. 17 and 18, respectively. Note that planes slicing through WT2 and WT3 are neglected for the same reason as discussed earlier. Wake deficit is computed as the difference between the waked and ambient flow. Therefore, a negative value indicates the wake velocity is less than the freestream velocity. All of the FAST.Farm solutions have similar wake deficits, with slightly stronger deficits in FFARM_ABL than in the TurbSim-generated inflows.

V. Conclusions

The purpose of this study was to compare how synthetically generated inflow from TurbSim and LES-generated inflow predict turbine and wake response using FAST.Farm, and to set guidelines for producing TurbSim-generated inflow for use in FAST.Farm simulations. Three variations of TurbSim-generated inflow were compared to LES-generated inflow. Inflow tailoring with TurbSim included specifying the velocity time series at the upstream turbine hub height; specifying the velocity spectra using IEC standards and matching LES-generated inflow hub height velocity standard deviations; and repeating this process but reducing high-frequency energy content. All TurbSim-generated inflows used the mean vertical wind profile from the LES-generated inflow and generic IEC spatial-coherence models and parameters. The reduction of high-frequency energy content had a negligible effect on wake and turbine response because wake meandering is based on low-pass filtering of the ambient flow field. Matching the inflow time series at the hub of the upstream turbine resulted in a better match of the turbine response time series for that turbine. However, turbine and wake response statistics for all turbines agree well without specifying a matching time series a priori. The lateral spatial

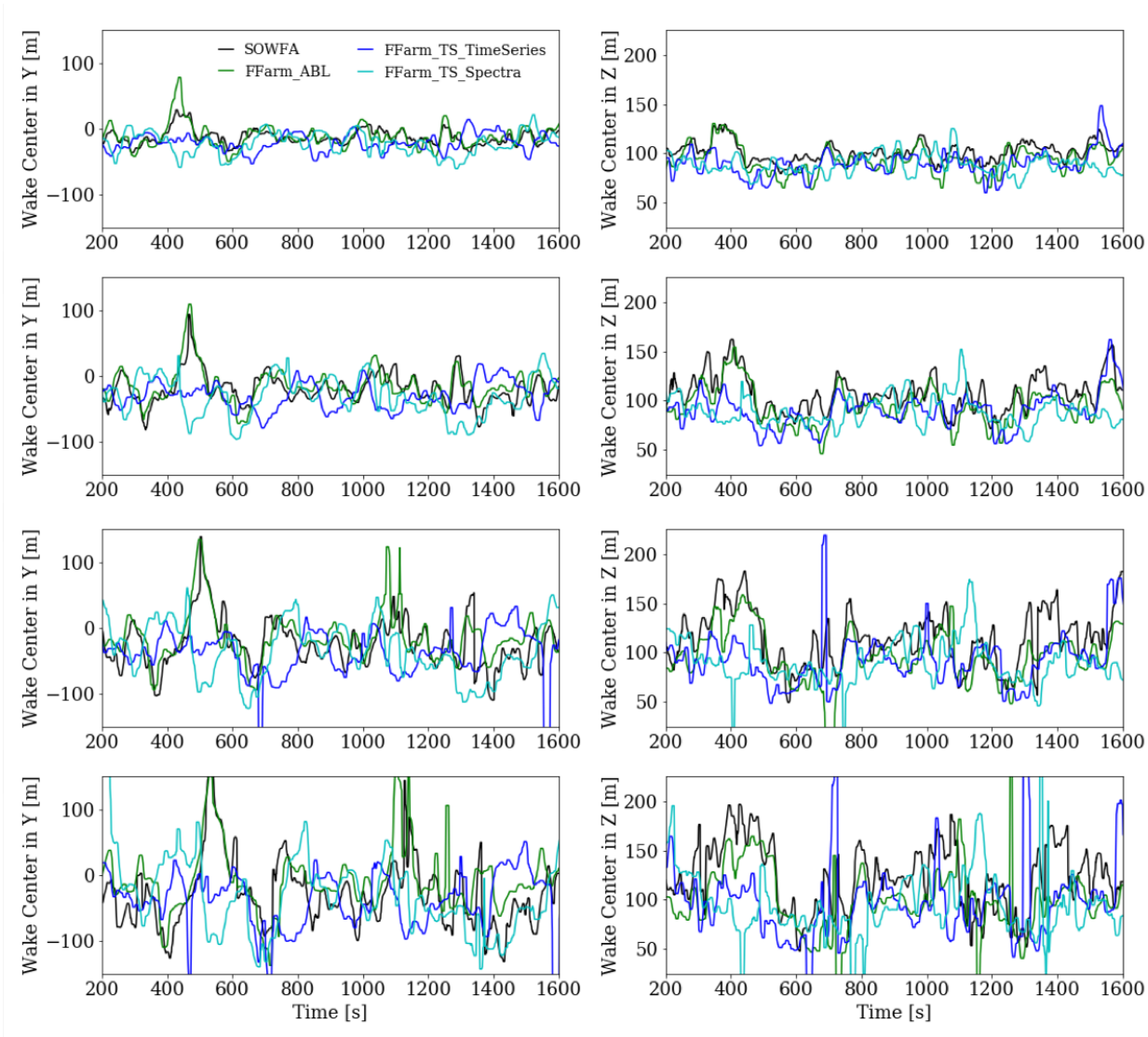

Fig. 14 Time series of lateral (left) and vertical (right) wake center positions between $2D$ and $8D$ downstream in $2D$ intervals (top to bottom) for Case V8_TI10_1WT_YAW.

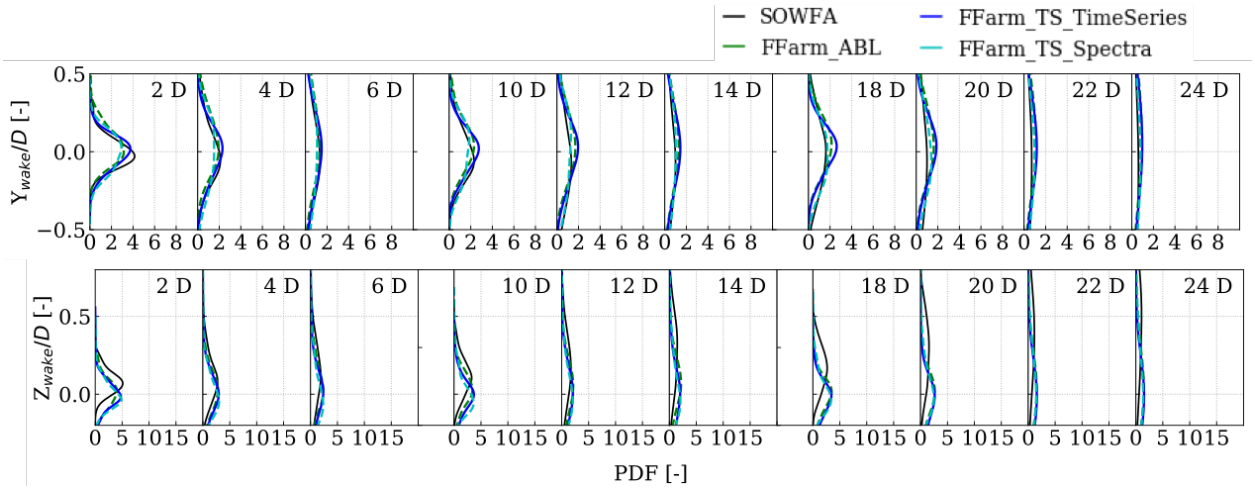

Fig. 15 PDF results of lateral (top) and vertical (bottom) wake center positions for Case V8_TI10_3WT.

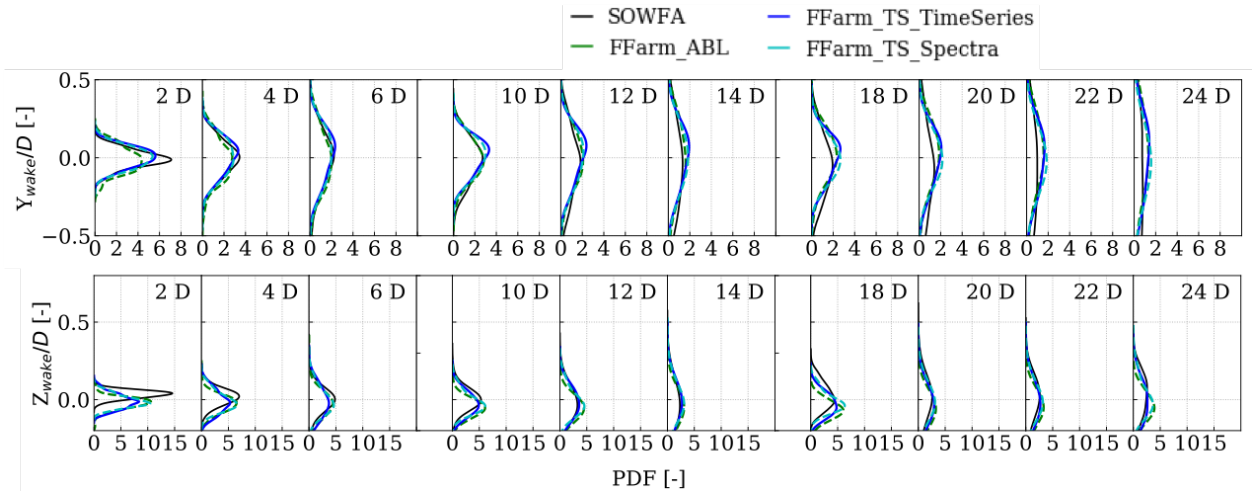

Fig. 16 PDF results of lateral (top) and vertical (bottom) wake center positions for Case V8_TI6_3WT.

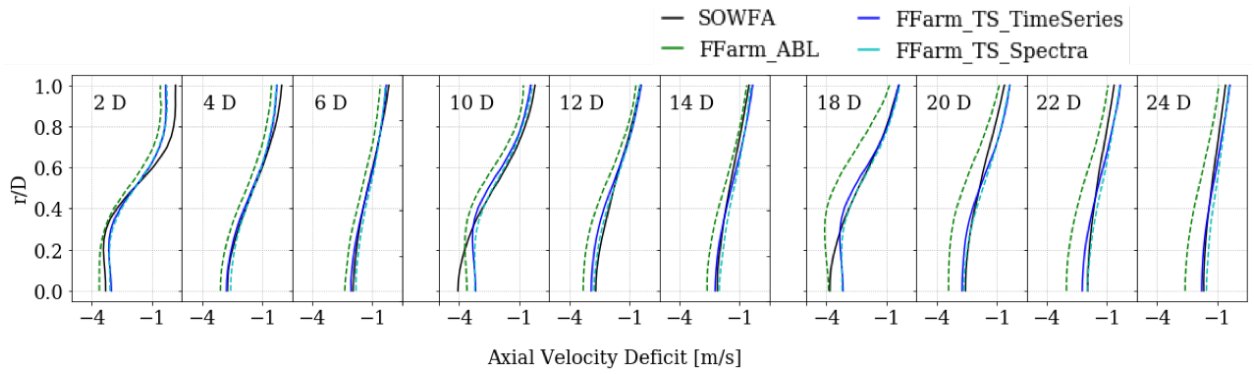

Fig. 17 Axial wake deficits in the meandering frame of reference for Case V8_TI10_3WT.

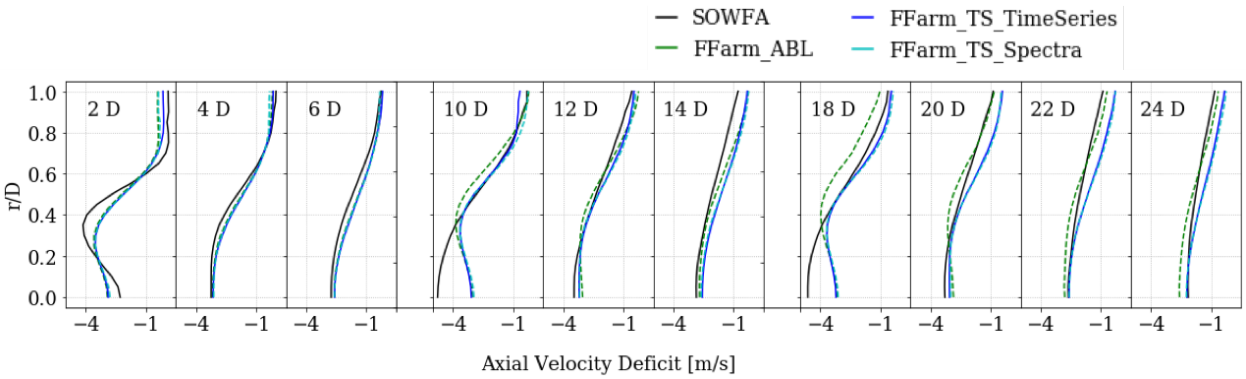

Fig. 18 Axial wake deficits in the meandering frame of reference for Case V8_TI6_3WT.

coherence of the v-and w-velocity components has been shown to be very important for accurately modeling of wake meandering. Further study of the impact of spatial coherence on wake meandering is warranted, as well as calibration of the coherence model parameters to LES coherence at low frequencies. Overall, all simulations compared well with high consistency between the inflow techniques. With proper setup, it is possible to use TurbSim-generated inflow with FAST.Farm to accurately predict turbine response and wake development in a wind farm setting.

Acknowledgments

This work was authored by the National Renewable Energy Laboratory, operated by Alliance for Sustainable Energy, LLC, for the U.S. Department of Energy (DOE) under Contract No. DE-AC36-08GO28308. Funding provided by the U.S. Department of Energy Office of Energy Efficiency and Renewable Energy Wind Energy Technologies Office. The views expressed in the article do not necessarily represent the views of the DOE or the U.S. Government. The U.S. Government retains and the publisher, by accepting the article for publication, acknowledges that the U.S. Government retains a nonexclusive, paid-up, irrevocable, worldwide license to publish or reproduce the published form of this work, or allow others to do so, for U.S. Government purposes.

References

[1] Doubrawa, P., Annoni, J., Jonkman, J., and et al., "Optimization-Based Calibration of FAST.Farm Parameters Against SOWFA," *AIAA SciTech Forum*, AIAA, Kissimmee, FL, 2018. doi:https://arc.aiaa.org/doi/pdf/10.2514/6.2018-0512.

[2] Jonkman, J., Doubrawa, P., Hamilton, N., and et al., "Validation of FAST.Farm Against Large-Eddy Simulations," EAWE, Milano, Italy, 2018.

[3] Jonkman, B., "TurbSim User's Guide v2.00.00," Tech. Rep. NREL/TP-xxxx-xxxxx, National Renewable Energy Laboratory, Golden, CO, October 2014.

[4] Larsen, G. C., Madsen, H. A., Thomsen, K., and et al., "Wake Meander: A Pragmatic Approach," *Wind Energy*, Vol. 11, 2008, pp. 337–95. doi:http://onlinelibrary.wiley.com/doi/10.1002/we.267/epdf.

[5] Jonkman, J., Annoni, J., Hayman, G., Jonkman, B., and purkayastha, A., "Development of FAST.Farm: A New MultiPhysics Engineering Tool for Wind-Farm Design and Analysis," *AIAA SciTech Forum*, AIAA, Grapevine, TX, 2017. doi:http://arc.aiaa.org/doi/pdf/10.2514/6.2017-0454.

[6] Jonkman, J. M., "FAST.Farm User's Guide and Theory Manual," Tech. Rep. NREL/TP-xxxx-xxxxx, National Renewable Energy Laboratory, Golden, CO, Unpublished 2018.

[7] Churchfield, M. J., Moriarty, P. J., Martinez, L. A., and et al., "A Large-Eddy Simulation of Wind-Plant Aerodynamics," AIAA, Nashville, TN, 2012. doi:http://dx.doi.org/10.2514/6.2012-537.

[8] Jonkman, J., Butterfield, S., Musial, W., and Scott, G., "Definition of a 5-MW Reference Wind Turbine for Offshore System Development," Tech. Rep. NREL/TP-500-38060, National Renewable Energy Laboratory, Golden, CO, February 2009.

[9] 61400-1, I., "Wind Turbines - Part 1: Design Requirements," Tech. Rep. 3rd edition, International Electrotechnical Commission, Geneva, Switzerland, March 2006.

[10] Quon, E., "SAMWICH Wake-Tracking Toolbox," `https://github.com/ewquon/waketracking`, 2017.